PHYSICAL REVIEW B **80**, 205316 (2009)

Role of electronic excitations in the energy loss of H_2^+ projectiles in high-κ materials

S. M. Shubeita, R. C. Fadanelli, J. F. Dias, and P. L. Grande
Instituto de Física, Universidade Federal do Rio Grande do Sul, Avenida Bento Gonçalves 9500, 91501-970 Porto Alegre, RS, Brazil

C. D. Denton and I. Abril
Departament de Física Aplicada, Universitat d'Alacant, Apartat 99, E-03080 Alacant, Spain

R. Garcia-Molina
Departamento de Física-CIOyN, Universidad de Murcia, Apartado 4021, E-30080 Murcia, Spain

N. R. Arista
División Colisiones Atómicas, Centro Atómico Bariloche, Instituto Balseiro, RA-8400 San Carlos de Bariloche, Río Negro, Argentina
(Received 7 August 2009; revised manuscript received 19 October 2009; published 18 November 2009)

In the present work we report on the energy loss ratio R_n of fast H_2^+ clusters in thin films (30–50 Å) of $LaScO_3$ and HfO_2. The medium energy ion scattering technique was employed covering a broad energy range (40–200 keV/amu). The energy loss ratio data showed no clear evidence of collective excitations in these materials. The experimental results were interpreted in terms of three different theoretical approaches: the dielectric formalism with the Brandt-Reinheimer theory for semiconductor materials; the detailed simulation of the molecular fragments dynamics through the target; and finally the unitary convolution approximation adapted for hydrogen molecules. Only the simulation agrees with the experimental results for both oxides. The unitary convolution approximation works quite well for HfO_2 but overestimates slightly the $LaScO_3$ data. The overall results indicate that the energy loss ratio depends critically on the description of the electronic properties of such oxides.

DOI: 10.1103/PhysRevB.80.205316 PACS number(s): 79.20.Ap, 34.50.Bw, 34.10.+x, 36.40.−c

I. INTRODUCTION

The energy loss of keV ions in matter is dominated by inelastic collisions with valence electrons, which can lead to electron-hole pair excitations and to a collective electronic motion known as plasmon excitation. As far as ions are concerned, plasmons can be understood as the response of the electronic medium to a quick change or sudden oscillation of the electric-field induced by the passage of a fast ion. Plasmon excitations are characterized by a plasma frequency ω_p and present different aspects whether bulk, surface, or interfaces are considered.[1–3] For heavy charged particles, the ion velocity threshold for plasmon excitation is approximately 1.3 times the Fermi velocity.[2] Moreover, plasmons cannot be singled out directly from typical transmission experiments. In this case, intrinsic multiple small-angle scattering events obfuscate the effects due to plasmon excitations[2] and no particular structures were ever observed in ion energy loss spectra around the plasmon threshold energy.[4]

Although the measurement of the energy distribution of scattered electrons during ion bombardment proved to be a useful technique in the study of electronic excitations,[2,5–7] a different method employing hydrogen cluster projectiles and high energy resolution backscattering measurements were used to determine the onset of long-range collective electronic excitations in SiO_2.[8] In this case the underlying mechanism is the vicinage effect,[9,10] which is related to the pattern generated by the interference of the wake potentials created by the moving particles. Taking into account that the plasmon cross section is very sensitive to this interference pattern,[8] the use of hydrogen molecules becomes a natural choice for the study of long-range electronic excitations with ions.

The energy loss ratio R_n of a swift molecule is given by

$$R_n = \frac{\Delta E_{\text{molecule}}}{\sum_{i=1}^{n} \Delta E_i}, \tag{1}$$

where ΔE stands for the energy loss and n is the number of atoms making up the molecule. When the internuclear distances r_0 among the molecular fragments are large, they move in an uncorrelated manner and R_n is close to 1. On the other side, for small r_0, R_n can be quite different from 1, giving rise to the so called "vicinage effects" in the energy loss. The Coulomb explosion[11] tends to increase r_0 and the width of the energy loss distribution, the latter having little impact on the mean energy loss in amorphous media.[12,13] That makes its contribution to the energy loss ratio R_n relatively small. On the other hand, the interference effect arising from the superposition of wake potentials is dependent on the internuclear distances of the fragments and can contribute directly to the energy loss of the fragments. Therefore, the ratio R_n will depend largely on the interference effect and, to a much lesser degree, on the Coulomb explosion as far as ultrathin films are concerned.

Different techniques employing ionic clusters have been used in the study of energetic molecules interacting with matter under channeling[12,14–17] and random[9,10,18,19] orientations, providing a deeper insight on the Coulomb explosion and interference effects. In particular, the Coulomb explosion imaging method[18,19] is the only one among them to provide structural information of individual molecules. All these techniques rely on durable targets and several inconsistencies

reported in the literature are related to target degradation during ion irradiation.[20] Moreover, the target thickness plays a key role in the experiments and may hamper the interpretation of results related to fundamental physical processes. For instance, multiple scattering within the target is an inherent process in the ion-matter interaction and becomes more severe as the target thickness increases. These events tends to change the dynamics of the fragments, and in Coulomb explosion experiments it can lead to distortions if not taken into account accordingly.[21]

Quite recently, high energy resolution backscattering experiments provided the first direct evidence of plasmon excitations induced by H_2^+ and H_3^+ molecules interacting with very thin SiO_2 films.[8] In this work we extend this investigation to high dielectric constant κ (Ref. 22) oxides such as HfO_2 and $LaScO_3$, which have recently gained considerable interest as possible gate oxides to replace SiO_2 in metal-oxide-semiconductor field-effect transistors.[23,24] To that end, we employ the same experimental technique described in Ref. 8 along with calculations obtained from both theory and simulations of the energy loss ratio R_n using a realistic description, when available, of the electronic properties of the above materials.

II. EXPERIMENTAL PROCEDURE

The targets employed in the experiments were deposited on crystal silicon following different procedures. The HfO_2 target was prepared by metalorganic chemical vapor deposition (MOCVD) of HfO_2 at 550 °C using Hf-*t*-butoxide.[25,26] The $LaScO_3$ film was deposited using a conventional molecular beam epitaxy chamber with a controlled admission of oxygen.[22,27] The final thickness achieved for HfO_2 and $LaScO_3$ films were 50 and 33 Å, respectively.

The experiments were carried out at the Ion Implantation Laboratory of the Physics Institute (Federal University of Rio Grande do Sul). A 500 kV electrostatic accelerator provided beams of H^+ and H_2^+ clusters in the energy range between 40 and 200 keV/amu. The samples were mounted on a three-axis goniometer inside the reaction chamber kept under a pressure of about 10^{-7} mbar. Typical currents for H^+ and H_2^+ beams were 15 and 8 nA, respectively.

The high energy resolution backscattering experiments were performed using the MEIS (medium energy ion scattering) technique.[28] A fraction of backscattered protons emerging from the target are analyzed in the toroidal electrostatic analyzer (TEA) mounted at 120° with respect to the beam direction. At the top end of the TEA a set of two microchannel plates coupled to a position-sensitive detector allow each ion to be energy- and angle-analyzed leading to two-dimensional (2D) spectra. The TEA angular aperture is 30° and each angle bin corresponds to 0.08°. The overall energy resolution of the system is 350 eV.

Details of the data analysis are found in Ref. 8. In short, the 2D spectrum has to be projected onto the energy axis for a particular set of angle bins in order to allow the adequate processing of the information contained in them. To improve the counting statistics, a total of 50 angle bins are assembled together, corresponding to an angular window of 4°. Finally, three different angular windows of 4° each are selected, yielding three one-dimensional (1D) energy spectra for each experiment. It is important to bear in mind that each step of this procedure includes proper corrections that take into account the different kinematical factors associated to each angle bin and the depth where the backscattering event took place.

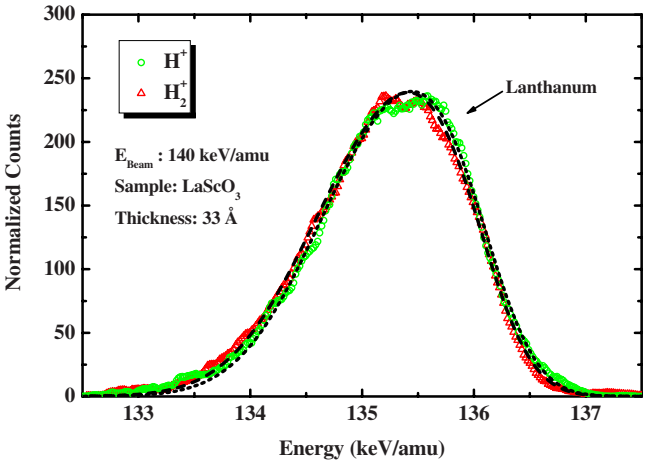

FIG. 1. (Color online) Typical 1D energy spectra obtained for H^+ and H_2^+ projectiles impinging on a $LaScO_3$ film. Both peaks represent those particles backscattered in lanthanum. The beam energy is 140 keV/amu and the film thickness is 33 Å. Dash and dotted lines (details in the text) are the best fits provided by the SIMULMEIS code (Ref. 8) for H^+ and H_2^+ spectra, respectively.

As an example we show in Fig. 1 typical 1D energy spectra obtained for 140 keV/amu H^+ and H_2^+ projectiles interacting with a 33 Å thick $LaScO_3$ film. The broad peaks represent those particles backscattered in La and were normalized for a better assessment of the results. A comparison between the results reveals that both spectra have approximately the same width, indicating that their energy loss is about the same.

In order to analyze the 1D spectra we used the simulation code for 1D MEIS spectra (SIMULMEIS).[8] In short, this code calculates the probability of detecting an ion with a final energy E_f backscattered at a particular depth within the target assuming a Gaussian distribution for the backscattered particles. The effect of the energy loss in the backscattering collision is calculated according to Ref. 29. In this code, all experimental factors and physical properties of the target such as structure (bulk or layered), thickness, density and atomic composition serve as input parameters. The mean energy loss and its variance along the incoming and outgoing trajectories are used as input parameters as well. The free parameters in the simulations are the target thickness, the energy loss and the straggling. For the proton case, the values assumed for the energy loss and straggling were allowed to vary in a restricted range around those obtained from the SRIM 2008 code[4] and the straggling theory developed by Chu.[30] In addition, we have also considered a depth dependent straggling due to the Coulomb explosion. For the analysis of spectra generated by H_2^+ clusters, these parameters were kept fixed and only the energy loss ratio R_2 and overall resolution (because of its enlargement due to the Coulomb

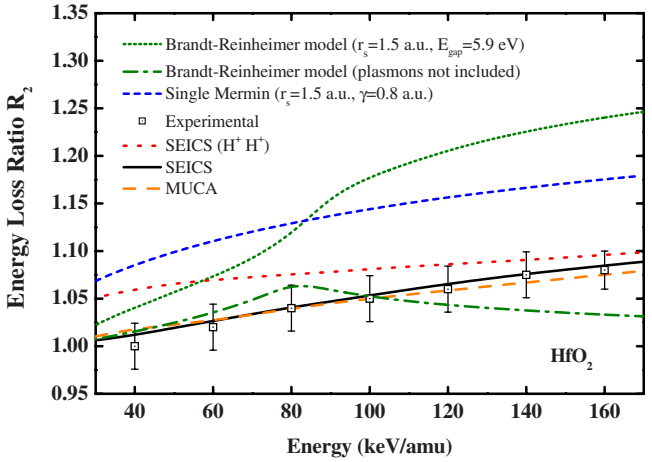

FIG. 2. (Color online) The experimental energy loss ratio R_2 (squares) for HfO_2 as a function of the incident cluster energy. The short-dashed line represents the results of the dielectric formalism using a single Mermin dielectric function. The continuous line represents the results of the simulations using the SEICS code. The dotted line represents the results of the simulations using the SEICS code for protons fragments only. The short-dotted line represents the results of the Brandt-Reinheimer theory. All these calculations include plasmon excitations. The dash-dotted line represents the results of the Brandt-Reinheimer theory not including plasmon excitations. The dashed line represents the results obtained by MUCA calculations. See text for further details.

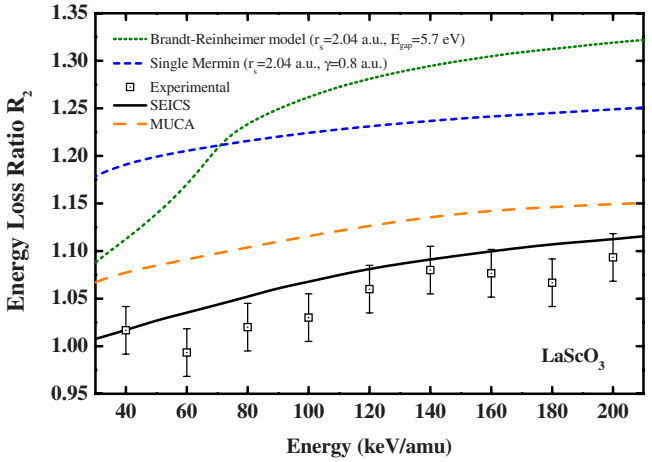

FIG. 3. (Color online) The same as Fig. 2 but for $LaScO_3$.

explosion of the molecule) were allowed to vary in order to obtain the best fit of the respective energy spectra (see dash and dotted lines in Fig. 1).

The final results and respective uncertainties for the energy loss ratios R_2 shown in this work were evaluated in the following way: (i) one measurement was carried out for each cluster energy; (ii) for each measurement, three 1D spectra were obtained; (iii) each 1D spectrum yielded one energy loss ratio, whose uncertainty was evaluated by changing the values of the stopping parameters and checking the goodness of the result; (iv) all energy loss ratio values were averaged; and (v) the uncertainties from steps (iii) and (iv) were convoluted, yielding the uncertainties quoted in Figs. 2 and 3, which will be discussed in Sec. IV.

III. CALCULATIONS

We carried out calculations of the energy loss ratio R_2 using three independent approaches: (i) the dielectric formalism;[10] (ii) simulations using the simulation of energetic ions and clusters through solids (SEICS) code[13,31] and (iii) the unitary convolution approximation,[32] which was recently adapted for the case of cluster projectiles.[33] The first two approaches are based on a realistic description of the target electronic response, while the latter provides information about higher-order effects.

The calculations with the dielectric formalism were made using two different models: (a) the Brandt-Reinheimer model and (b) a single Mermin dielectric function model. The Brandt-Reinheimer model[34] is an extension of the Lindhard-Winther approach (for free electrons) which includes the effect of an energy gap and the corresponding redistribution of the oscillator strengths. It is a quantum mechanical model that includes two types of excitations: individual electrons and plasmons. However, it does not include the effect of damping of the plasmon excitations. The only two parameters in this model are the Wigner-Seitz radius r_s and the energy gap E_{gap}. The present calculations were made using r_s=1.5 a.u. and E_{gap}=5.9 eV for HfO_2, and r_s=2.04 a.u. and E_{gap}=5.7 eV for $LaScO_3$. The single Mermin model[35] is a dielectric approach based on a fit of the energy loss function (ELF) in the optical limit using available experimental data from previous sources. In this case the model parameters are the Wigner-Seitz radius r_s, the energy gap E_{gap}, and the damping factor γ. The present calculations were made with r_s=1.5 and 2.04 a.u., E_{gap}=5.9 and 5.7 eV, and γ=0.8 a.u., for HfO_2 and $LaScO_3$, respectively.

The second approach was done using the SEICS code,[13,31] which simulates the trajectories of the molecular constituents inside the target. The code incorporates the stopping forces on each fragment including also the energy loss straggling. These forces were calculated using the dielectric formalism and the MELF-GOS model[36,37] to account for the electronic target response. Briefly, the MELF-GOS model describes the response of the outer-shells electrons by fitting the experimental ELF in the optical limit with Mermin-type ELFs (Ref. 35) and the response of the inner-shell electrons with generalized oscillator strengths (GOS).[38] In the present study, up to 7 Mermin-type ELFs were necessary in order to fit the excitation spectrum for HfO_2.[39,40] The experimental ELF for $LaScO_3$ was obtained from optical experiments of reflectivity[41] using a Kramers-Kronig analysis, and up to 10 Mermin-type ELFs were used in the fitting. The wake forces between fragments, which are the main responsible for the vicinage effects in the energy loss, are also implemented in the code using the dielectric formalism and the same method to account for the ELF.[36] Furthermore, the program also includes the Coulomb repulsion between the fragments and the multiple elastic scattering with the target nuclei through a Monte Carlo sampling. The charge exchange of the projectile was treated by calculating the free paths between successive capture or loss events, using a simple model for the loss cross sections and the charge fractions given by the CasP

code.[42] The H_2^+ molecules are chosen initially to be in random orientation and with an interatomic distance distribution according to Ref. 9. The first two approaches include binary (electron-hole) and plasmon excitations in the calculations.

The higher-order effects in the vicinage effect were estimated using the molecular unitary convolution approximation (MUCA) and the molecular perturbative convolution approximation (MPCA).[33] The MPCA approximation is based on the first-order Born approximation while the MUCA includes higher-order effects. The impact-parameter dependent energy loss $Q(b)$ was evaluated for each ion velocity using the atomistic description of the target according to the Hartree-Fock-Slater method.[43] In addition, $Q(b)$ was averaged over all molecular orientations and integrated over all impact parameters to obtain the stopping cross section for the cluster projectiles. The same approach was performed for the monoatomic energy loss.[32] In order to evaluate the contribution of multiple scattering to the energy loss ratio R_2, a Monte Carlo simulation was developed to calculate the mean internuclear distance between the H_2^+ fragments after passing through the films. In short, a Molière screening potential[44] is used to describe the interaction with the target atoms, which are randomly distributed according to the known atomic densities. Newton's equations are then solved considering the forces between the fragments and the target nuclei. The angles between the molecular axis and the motion direction, as well as the initial grid position of the projectile impinging the target, are chosen randomly. The fragment charge state is kept constant (according to Ref. 45) along the entire ion path and the Molière potential screening parameter is evaluated accordingly. In order to describe the initial distances between the H_2^+ fragments, we have followed the procedure outlined in Ref. 46. In that work, the initial distance is chosen randomly from a Gaussian distribution with a mean value of 1.17 Å and a width of 0.3 Å. Finally, the interaction between the H_2^+ fragments is modeled using a Yukawa potential where the screening distance is given by v/ω_p, with v being the projectile fragment velocity and ω_p the target plasmon frequency. The ω_p values adopted in this work were obtained directly from the r_s values.

IV. RESULTS AND DISCUSSION

The experimental energy loss ratios R_2 for H_2^+ projectiles impinging on HfO_2 and $LaScO_3$ are shown by symbols (with error bars) in Figs. 2 and 3, respectively. In general, both results display minor interference effects since the energy loss ratios are close to unity. For $LaScO_3$ a slight increase in the R_2 values occurs above 120 keV/amu, indicating that at these energies about 7% of the energy loss is due to interference effects between the fragments after break up. The results for HfO_2 shown in Fig. 2 are similar to those obtained for $LaScO_3$ but display a steady and smooth increase over the entire energy range studied in this work. The overall picture for both dielectric materials differs significantly from previous results published for silicon dioxide where a clear signature of plasmon excitations with substantial contribution of interference effects to the energy loss ratios was reported.[8]

The theoretical calculations for the stopping ratio R_2 employing a single Mermin dielectric function are also displayed in Figs. 2 and 3. For HfO_2 such calculations strongly overestimate in an almost constant value the experimental data in the whole energy range under study. Considering the Brandt-Reinheimer theory, the calculations including plasmon excitations overestimate the experimental results in different magnitudes in the whole energy range under study, being closer to the experimental data at low energies and farther at high energies. On the other hand, the results from the SEICS code, which properly takes into account the main interactions felt by the molecular fragments and uses a realistic excitation spectrum of the HfO_2 target, provide a very good agreement with experiments. Finally, according to our simulations, multiple scattering plays a minor role in the energy loss process.

The same trend observed for HfO_2 can be found for $LaScO_3$ (Fig. 3) where the calculations using a single Mermin or Brandt-Reinheimer theory overestimate substantially the experimental data in the whole energy range. For comparison purposes, Fig. 2 shows the Brandt-Reinheimer theory without plasmon excitations as well. These results show the importance of the plasmon excitations in this theory for energies higher than 80 keV/amu for HfO_2. A similar behavior occurs for $LaScO_3$, but in a different threshold energy.

The main reason for the small and relatively smooth increase of the energy loss ratio observed in Figs. 2 and 3 stems from the complex electronic structure of such oxides. In fact, unlike other materials such as C and SiO_2 where a dominant long-range electronic excitation is present, these complex oxides have several and equally important excitation energies (mix of plasmon excitations, excitons, and interband transitions). They lead to different onset projectile energies, which explains the smoothly increase in energy loss ratio. In addition, these materials have a much larger plasmon-excitation energy (of about 30 eV for HfO_2),[47] which reduces the overall vicinage effect. It is important to note that the shape of the wake potential obtained from the use of a sum of Mermin-type ELF's is similar to the one from a single Mermin with a large damping factor γ. Nevertheless the vicinage effects, which depend on the relation between the wake forces and the stopping forces, are quite different in both models.

The nuclear multiple scattering is the responsible for most of the internuclear separation inside the target. For instance, when 100 keV/amu H_2^+ molecular ions impinge on 50 Å thick HfO_2 foils, multiple scattering increases the average internuclear distance from $r_0=1.28$ Å to $r_0=1.69$ Å. Nevertheless, the effect of this distance increase on R_2 is small (not shown in Fig. 2).

The results of the molecular unitary convolution approximation MUCA are also shown in Figs. 2 and 3. The perturbative approach MPCA (not shown in Figs. 2 and 3) yields nearly the same results provided by MUCA, which means that no significant higher-order effects are at play. For the $LaScO_3$, the results obtained by MUCA slightly overestimates the experiment in the whole energy range studied. Furthermore, the rather good agreement between experiment and theory for HfO_2 might be accidental since no proper electronic excitations of the target were considered. As a

matter of fact, a closer look at the absolute stopping powers provided by MUCA reveals a discrepancy with the experimental stopping powers. That means that the MUCA approach is not fully suitable for materials with complex electronic excitations. However, an atomic description of the target as used by MUCA may work well for the calculations of the energy loss ratio since it depends more on the broadness of the electronic excitation spectrum than their precise values.

The charge state of the fragments inside the solid is considered since the vicinage effect is smaller in the case of both fragments having neutral charge (H^0). In the present simulations (SEICS and MUCA) the charge state of any fragment at a given time is calculated using simple models for loss cross sections and the equilibrium values of charge fractions as given by the CasP code.[42] We did not consider vicinage effects in the charge state. Therefore, the following products can occur after molecular breakup: H^+H^+, H^+H^0, and H^0H^0. The inclusion of charge states in the calculation tends to decrease the energy loss ratio values even further at lower energies, where more neutrals H^0 are formed. Indeed, as shown in Fig. 2, a calculation considering H^+H^+ only would yield higher energy loss ratios.

V. CONCLUSIONS

In this work we investigated the energy loss ratio values for H_2^+ molecules interacting with thin HfO_2 and $LaScO_3$ films. Contrary to light oxides such as SiO_2, the present experimental data indicate that the vicinage effect plays a minor role in the process. This is a direct consequence of the electronic properties of these systems. In fact, their description by using a sum of Mermin-type dielectric functions, which reproduce the valence-band properties, smear out the vicinage effect over the projectile energies and thus no clear onset for long-range electronic excitations were observed. Moreover, although effects such as multiple scattering tend to increase the internuclear distance for the present thin films, they play a negligible role in the observed energy loss ratio.

ACKNOWLEDGMENTS

This research was supported by Conselho Nacional de Desenvolvimento Científico e Tecnológico (CNPq), Fundação de Amparo à Pesquisa do Estado do Rio Grande do Sul (FAPERGS), the Spanish Ministerio de Educación y Ciencia (Projects No. FIS2006-13309-C02-01 and No. FIS2006-13309-C02-02 and support under the Ramón y Cajal Program). The authors would like to thank J. M. J. Lopes of Institute for Bio- and Nanosystems (IBN1-IT) and Center of Nanoelectronic Systems for Information Technology (CNI), Research Center Juelich, Juelich, Germany, for the $LaScO_3$ sample.

[1] H. Raether, *Excitation of Plasmons and Interband Transitions by Electrons* (Springer-Verlag, Berlin, 1980).
[2] R. A. Baragiola, C. A. Dukes, and P. Riccardi, Nucl. Instrum. Methods Phys. Res. B **182**, 73 (2001).
[3] M. Rocca, Surf. Sci. Rep. **22**, 1 (1995).
[4] J. F. Ziegler, J. P. Biersack, and U. Littmark, *The Stopping and Range of Ions in Solids* (Pergamon Press, New York, 1985). The SRIM code is available at www.srim.org.
[5] S. M. Ritzau, R. A. Baragiola, and R. C. Monreal, Phys. Rev. B **59**, 15506 (1999).
[6] E. A. Sanchez, J. E. Gayone, M. L. Martiarena, O. Grizzi, and R. A. Baragiola, Phys. Rev. B **61**, 14209 (2000).
[7] N. J. Zheng and C. Rau, J. Vac. Sci. Technol. A **11**, 2095 (1993).
[8] S. M. Shubeita, M. A. Sortica, P. L. Grande, J. F. Dias, and N. R. Arista, Phys. Rev. B **77**, 115327 (2008).
[9] W. Brandt, A. Ratkowski, and R. H. Ritchie, Phys. Rev. Lett. **33**, 1325 (1974).
[10] N. R. Arista, Nucl. Instrum. Methods Phys. Res. B **164-165**, 108 (2000).
[11] D. S. Gemmell, J. Remillieux, J. C. Poizat, M. J. Gaillard, R. E. Holland, and Z. Vager, Phys. Rev. Lett. **34**, 1420 (1975).
[12] R. C. Fadanelli, P. L. Grande, M. Behar, J. F. Dias, K. Czerski, and G. Schiwietz, Phys. Rev. B **73**, 245336 (2006).
[13] R. Garcia-Molina, C. D. Denton, I. Abril, and N. R. Arista, Phys. Rev. A **62**, 012901 (2000).
[14] J. M. Caywood, T. A. Tombrello, and T. A. Weaver, Phys. Lett. **37A**, 350 (1971).
[15] J. C. Poizat and J. Remillieux, J. Phys. B **5**, L94 (1972).
[16] T. A. Tombrello and J. M. Caywood, Phys. Rev. B **8**, 3065 (1973).
[17] V. A. Khodyrev, V. S. Kulikauskas, and C. Yang, Nucl. Instrum. Methods Phys. Res. B **195**, 259 (2002).
[18] Z. Vager, R. Naaman, and E. P. Kanter, Science **244**, 426 (1989).
[19] L. Lammich, H. Buhr, H. Kreckel, S. Krohn, M. Lange, D. Schwalm, R. Wester, A. Wolf, D. Strasser, D. Zajfman, Z. Vager, I. Abril, S. Heredia-Avalos, and R. Garcia-Molina, Phys. Rev. A **69**, 062904 (2004).
[20] A. R. Nyaiesh, W. Steckelmacher, and M. W. Lucas, J. Phys. C **11**, 2917 (1978).
[21] D. Zajfman, T. Graber, E. P. Kanter, and Z. Vager, Phys. Rev. A **46**, 194 (1992).
[22] J. M. J. Lopes, U. Littmark, M. Roeckerath, St. Lenk, J. Schubert, S. Mantl, and A. Besmehn, J. Appl. Phys. **101**, 104109 (2007).
[23] T. Heeg, M. Wagner, J. Schubert, Ch. Buchal, M. Boese, M. Luysberg, E. Cicerrella, and J. L. Freeouf, Microelectron. Eng. **80**, 150 (2005).
[24] M. Leskelä and M. Ritala, J. Solid State Chem. **171**, 170 (2003).
[25] K. P. Bastos, J. Morais, L. Miotti, R. P. Pezzi, G. V. Soares, I. J. R. Baumvol, R. I. Hegde, H. H. Tseng, and P. J. Tobin, Appl. Phys. Lett. **81**, 1669 (2002).
[26] R. P. Pezzi, J. Morais, S. R. Dahmen, K. P. Bastos, L. Miotti, G. V. Soares, I. J. R. Baumvol, and F. L. Freire, Jr., J. Vac. Sci. Technol. A **21**, 1424 (2003).
[27] J. M. J. Lopes, M. Roeckerath, T. Heeg, U. Littmark, J. Schubert, S. Mantl, Y. Jia, and D. G. Schlom, Microelectron. Eng. **84**,

1890 (2007).
[28] R. M. Tromp, H. H. Kersten, E. Granneman, R. Koudijs, and W. J. Kilsdonk, Nucl. Instrum. Methods Phys. Res. B **4**, 155 (1984).
[29] P. L. Grande, A. Hentz, R. P. Pezzi, I. J. R. Baumvol, and G. Schiwietz, Nucl. Instrum. Methods Phys. Res. B **256**, 92 (2007).
[30] W. K. Chu, Phys. Rev. A **13**, 2057 (1976).
[31] S. Heredia-Avalos, R. Garcia-Molina, and I. Abril, Phys. Rev. A **76**, 012901 (2007).
[32] G. Schiwietz and P. L. Grande, Nucl. Instrum. Methods Phys. Res. B **153**, 1 (1999).
[33] R. C. Fadanelli, P. L. Grande, and G. Schiwietz, Phys. Rev. A **77**, 032902 (2008).
[34] W. Brandt and J. Reinheimer, Phys. Rev. B **2**, 3104 (1970).
[35] N. D. Mermin, Phys. Rev. B **1**, 2362 (1970).
[36] I. Abril, R. Garcia-Molina, C. D. Denton, F. J. Pérez-Pérez, and N. R. Arista, Phys. Rev. A **58**, 357 (1998).
[37] S. Heredia-Avalos, R. Garcia-Molina, J. M. Fernández-Varea, and I. Abril, Phys. Rev. A **72**, 052902 (2005).
[38] R. F. Egerton, *Electron Energy-Loss Spectroscopy in the Electron Microscope* (Plenum Press, New York, 1989).
[39] J. Frandon, B. Brousseau, and F. Pradal, Phys. Status Solidi B **98**, 379 (1980).
[40] I. Abril, M. Behar, R. Garcia-Molina, R. C. Fadanelli, L. C. C. M. Nagamine, P. L. Grande, L. Schünemann, C. D. Denton, N. R. Arista, and E. B. Saitovitch, Eur. Phys. J. D **54**, 65 (2009).
[41] T. Arima and Y. Tokura, J. Phys. Soc. Jpn. **64**, 2488 (1995).
[42] P. L. Grande and G. Schiwietz, Phys. Rev. A **58**, 3796 (1998)
[43] F. Herman and S. Skillmann, *Atomic Structure Calculations* (Prentice-Hall, Englewood Cliffs, NJ, 1963).
[44] V. G. Molière, Z. Naturforsch. **2a**, 133 (1947).
[45] G. Schiwietz and P. L. Grande, Nucl. Instrum. Methods Phys. Res. B **175-177**, 125 (2001).
[46] D. Zajfman, Phys. Rev. A **42**, 5374 (1990).
[47] J. M. Sanz, M. A. Bañon, E. Elizalde, and F. Yubero, J. Electron Spectrosc. Relat. Phenom. **48**, 143 (1989).